Desorption induced formation of low-density GaN quantum dots: nanoscale correlation of structural and optical properties

OPEN ACCESS
IOP Publishing
Journal of Physics D: Applied Physics
J. Phys. D: Appl. Phys. **55** (2022) 145102 (7pp)
https://doi.org/10.1088/1361-6463/ac40b9

Desorption induced formation of low-density GaN quantum dots: nanoscale correlation of structural and optical properties

H Schürmann[1,*], G Schmidt[1], F Bertram[1], C Berger[1], S Metzner[1,2], P Veit[1], A Dadgar[1], A Strittmatter[1] and J Christen[1]

Institute of Physics, Otto-von-Guericke-University Magdeburg, 39106 Magdeburg, Germany

E-mail: Hannes.Schuermann@ovgu.de

Received 10 September 2021, revised 18 November 2021
Accepted for publication 7 December 2021
Published 5 January 2022

Abstract

We report on the formation process of GaN/AlN quantum dots (QDs) which arises after the deposition of 1–2 monolayers of GaN on an AlN/sapphire template followed by a distinct growth interruption (GRI). The influence of the duration of a GRI on the structural and optical properties of the GaN layer has been systematically investigated. QDs develop from initially bulky GaN islands, which nucleate in close vicinity to bundles of threading dislocations (TDs). For prolonged GRIs, a decreasing island size is observed which is consistent with a systematic blue shift of the emission wavelength. In addition, fragmentation of the bulky GaN islands into several smaller islands occurs, strongly dependent on local strain fields caused by TDs as well as on the different facet orientation of the islands. This morphological transition during GRI eventually leads to GaN QD formation, which assemble as clusters with a density of 10^8 cm^{-2}. Desorption of GaN is identified as the major source for this morphological transition. The GRI time allows for tuning of the QD emission wavelength in the ultraviolet spectral range.

Supplementary material for this article is available online

Keywords: quantum dots, gallium nitride, MOVPE, electron microscopy, cathodoluminescence spectroscopy

(Some figures may appear in color only in the online journal)

[2] Current affiliation: Research and Development, PROMECON GmbH, 39 179 Barleben, Germany.
[*] Author to whom any correspondence should be addressed.

1. Introduction

The realization of easy-to-use single photon generation is a critical issue for future quantum information technologies [1], such as key distribution in quantum communication [2] and quantum computing [3, 4]. In particular, for operation at elevated temperatures, GaN/AlN quantum dots (QDs) [5–7] are beneficial due to their high exciton binding energy [8]. Control of the size and shape of semiconductor QDs is implicitly required, since they have an immediate impact on the electronic and optical properties [9]. Low density QDs are favorable for deterministic mesa processing in order to achieve single photon emitting devices. Hence, understanding of the formation mechanism and its control is a prerequisite for the control and tunability of QD properties and spatial distribution.

In molecular beam epitaxy, growth of GaN QDs has been achieved by several methods such as Stranski–Krastanov (SK) epitaxy under N-rich conditions [10], post-growth ripening of N-rich grown SK QDs [11] and post-growth annealing of a Ga-rich grown GaN layer [12].

The growth of GaN/AlN QD structures by metal-organic vapor-phase epitaxy (MOVPE) is still challenging and has been realized by different approaches: silicon induced island formation due to its surfactant behavior was achieved by Tanaka *et al* [13]. Furthermore, low V/III ratios during the epitaxy of GaN have been used, which directly result in QD growth [14–16]. Another approach is the introduction of an annealing step after the deposition of a thin GaN layer [17]. Growing a GaN layer at higher temperatures with a subsequent growth interruption (GRI) leads to QD clusters nucleated at threading dislocations (TDs) with exceptionally narrow linewidths and clear single photon emission [18–20]. The cluster density was derived from atomic force microscopy (AFM) studies and is in the order of 10^8 cm^{-2}, which is promising for generating low density surfactant-free self-assembled GaN QDs by MOVPE. In this study, we focus on the investigation of the underlying formation mechanism and evolution of GaN QDs resulting from GRI after GaN deposition in MOVPE.

2. Methods

2.1. Sample growth

The samples were grown in an AIXTRON 200/4 RF-S MOVPE reactor on a 2″ *c*-plane AlN/sapphire template. After growth of a nominally 2 nm thick GaN layer at 960 °C with a V/III ratio of 30, the GaN QD formation was initiated by a subsequent GRI without ammonia and trimethylgallium supply. The GRI time was varied between 0 and 60 s. Subsequently, the GaN layer was capped with a 100 nm thick AlN layer.

2.2. Characterization

For spatially resolved analysis of the emission properties of the bulk samples, plan-view cathodoluminescence investigations were performed in a scanning electron microscope (SEM-CL) at $T = 9$ K. A beam current of 760 pA at 5 kV acceleration voltage leads to a steady-state occupation of two electron–hole pairs per QD assuming an average carrier lifetime of 0.5 ns [21, 22]. A detailed description of the SEM-CL setup is described in [23]. To analyze the optical properties of individual QDs, cross-sectional CL microscopy was performed directly in a scanning transmission electron microscope (STEM-CL) and was carried out at $T = 16$ K with 80 kV acceleration voltage. For further information about the STEM-CL setup, the reader is kindly referred to [24].

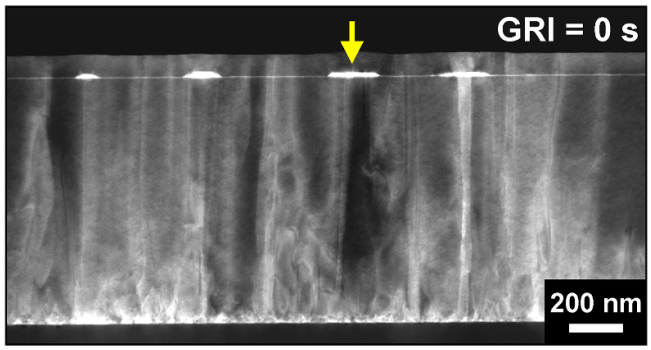

Figure 1. Cross sectional HAADF image of the reference sample with no GRI (arrow indicates one bulky GaN island).

3. Results and discussion

In figure 1 a cross-sectional high angle annular dark field image (HAADF) from transmission electron microscopy (TEM) analysis of the reference sample (0 s GRI) is displayed. In general, the HAADF signal is dominated by material contrast through thermal diffuse scattering [25]. The sapphire substrate shows up as a black contrast at the bottom of the image. It is followed in the vertical direction by the AlN buffer layer with a thickness of 920 nm. A TD density of 3×10^{10} cm^{-2} in the AlN buffer can be roughly estimated from this cross-sectional image. TDs commonly lead to high HAADF intensity due to de-channeling effects [26]. On top of the buffer, a continuous, (1.8 ± 0.7) nm thick GaN quantum well (QW) is formed (line of bright contrast in figure 1). Locally, distinct GaN accumulations are observed forming bulky islands with thicknesses of up to 19 nm and lateral extension above 100 nm (see yellow arrow). We find these bulky GaN islands preferentially in the vicinity of bundles of TDs. The resulting morphology of the GaN layer is directly passed through to the subsequently grown AlN cap. Thus, the shape, height, and density of the GaN islands can be estimated from atomic force microscopy of the capped sample surface (see supplementary material (available online at stacks.iop.org/JPD/55/145102/mmedia)). The density of these hexagonally shaped islands is only about 10^8 cm^{-2}.

Investigation of the cross-sectional HAADF image of the sample with 30 s GRI time (figure 2) reveals bright spots inside the GaN layer surrounded by a continuous GaN film as indicated by yellow arrows. The TD density is comparable to the

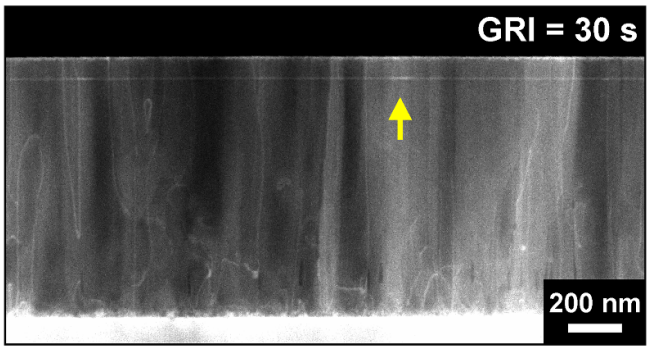

Figure 2. Cross sectional HAADF image of the sample 30 s GRI (arrow indicates one GaN island).

reference sample and the spots also have about the same density of around 10^8 cm^{-2} as the GaN islands in the reference sample as derived from AFM measurements on identically grown samples with 2 nm thin or without cap layers. This is further confirmed by analysis of several TEM images. Narrow optical emission lines could be assigned to these spots and some of these emission lines can be characterized as single photon emission lines [18]. Most strikingly, the thickness of the QW and islands is drastically reduced down to a few monolayers and (4.5 ± 0.7) nm, respectively. To explain the formation of these GaN QD clusters a systematic growth series has been investigated with the following results.

To visualize the evolution of the QD ensemble emission with GRI time, CL spectra of each sample were taken using plan-view scanning electron microscopy cathodoluminescence (SEM-CL) measurements (T = 9 K) averaging over an area of 10 × 15 μm^2 (see figure 3). The spectra are modulated by Fabry–Pérot thickness interferences. The Fabry-Perót interference order formula $m = 2n_{AlN}(\lambda_{Peak})d_{AlN}/\lambda_{Peak}$ yields a thickness of d_{AlN} = 0.9 µm consistent to STEM measurements. The wavelength dependent refractive index of AlN is obtained from [27]. A broad emission band centered at λ = 280 nm is observed for the reference sample (0 s GRI). The luminescence characteristics drastically change by introducing a GRI (i.e., 20 s GRI). Splitting into two different recombination channels occurs: a 280 nm emission band, which is attributed to the QD ensemble, as well as a high-energy shoulder at 240 nm wavelength identified as QW luminescence from the continuous GaN film. When the GRI time amounts to 30 s, the QW emission spectrally separates from the QD ensemble and shifts to 220 nm. Additionally, the QD emission band narrows and gets blueshifted. For t_{GRI} > 40 s, the QW emission vanishes and the QD ensemble CL narrows further. Here, the AlN near band edge (NBE) luminescence is additionally observed at 205 nm. Finally, the QD emission appears at 240 nm wavelength with a full width at half maximum of 231 meV for the longest GRI of 60 s.

More informative is the local variation of the emission characteristics, which allows us to map the temporal QD evolution during GRI. As a result, CL spectra have been acquired along a 2.5 μm line on the surface of each sample (figure 4). The emission of the reference sample has a broad

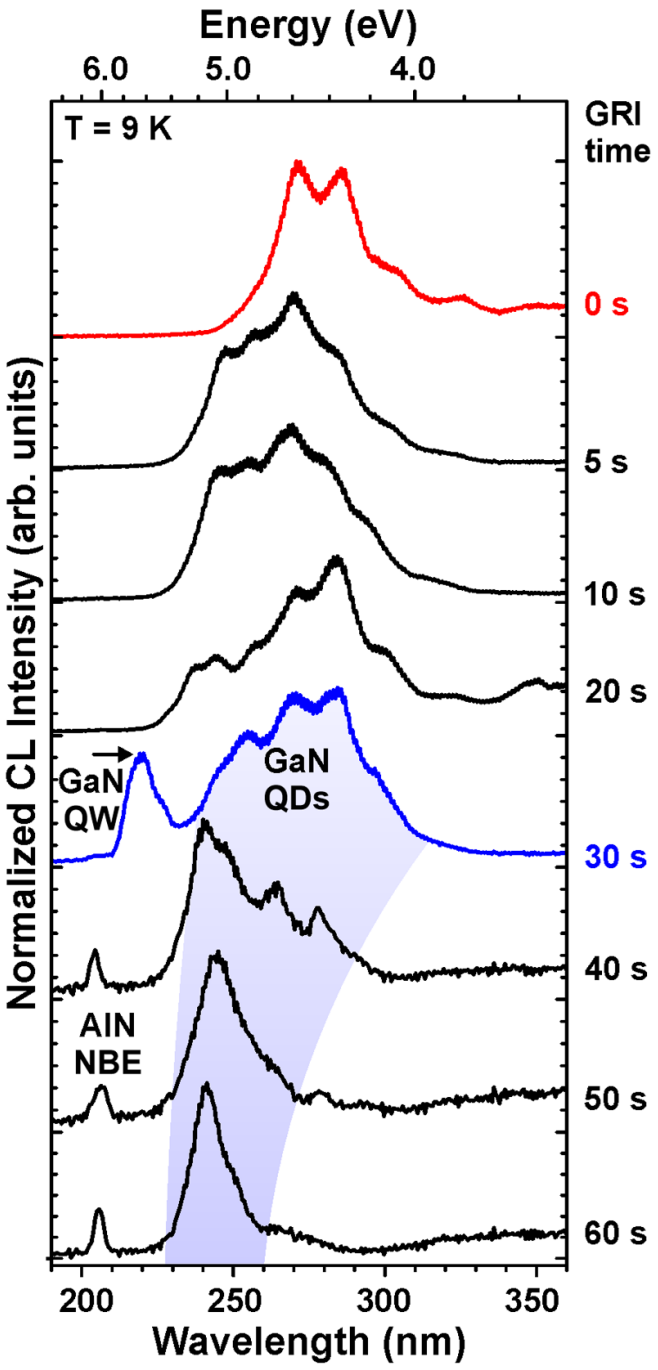

Figure 3. Spatially averaged plan-view SEM-CL spectra of the growth series with GRI times of 0–60 s taken at T = 9 K (normalized, vertically shifted). The GaN QD emission band (pale blue area) is clearly separated from the GaN QW for GRI > 20 s.

but homogeneous wavelength and intensity distribution along the linescan is only modulated by Fabry–Pérot interferences. The intensity varies between 50% (yellow contrast) and 100% (red contrast), whereas the emission center wavelength fluctuates about 28 nm. When introducing a short GRI, the intensity variations increase. After $t_{GRI} \geqslant 20$ s, the now distinguishable high energy QW luminescence is spectrally homogeneous at λ = 240 nm across the sample surface, whereas the QD emission band at λ > 250 nm exhibits strong local fluctuations in

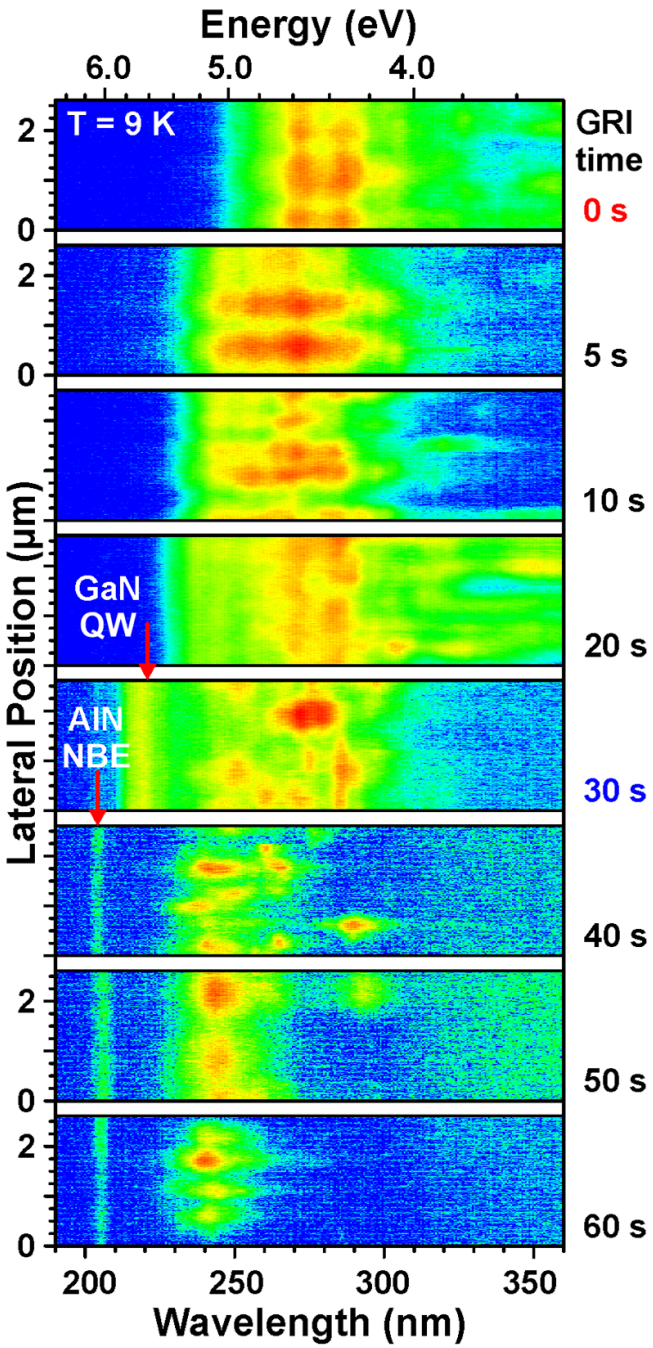

Figure 4. SEM-CL linescans in plan-view at $T = 9$ K show the spectrally and spatially resolved CL intensity distribution in a logarithmic scale over two orders of magnitude (blue—low intensity, red—high intensity) for each sample of the GRI growth series.

peak wavelength as well as in intensity. A GRI of 30 s results in distinctly separated QW and QD emission bands. The latter is a spotty emission band from 230 to 300 nm with various maxima. This indicates the presence of locally separated GaN QDs. For even longer GRIs, the GaN QW emission vanishes and the AlN NBE CL is persistent across the surface. After 40, 50 and 60 s of GRI, the number of intensity maxima within the 240 nm emission band decreases indicating the reduction of QD density with longer t_{GRI}. Only small QDs with the shortest emission wavelengths persist.

For a nano-scale one-to-one correlation of structural and local optical properties, scanning transmission electron microscopy cathodoluminescence (STEM-CL) images have been recorded in cross-section. A panchromatic CL intensity image of the reference sample (0 s GRI) is superimposed onto the simultaneously acquired HAADF image at 16 K (figure 5(a)). The CL intensity locally originates exclusively from the thin corrugated GaN film between the islands (figure 5(c)), whereas no emission from the bulky GaN islands is detected. This strongly indicates non-radiative recombination of the generated excess carriers within these islands. The corresponding CL spectrum integrated over the whole cross-section of figure 1 is shown in figure 5(b). The intense, broad emission of the GaN film between 250 and 360 nm is obtained together with the two characteristic broad defect related emission bands of the AlN buffer (Si-related at 330 nm and O-related at 420 nm) [28] (see also figure 6(d)).

For the direct comparison of continuous and interrupted growth after GaN QW epitaxy, the HAADF image and panchromatic STEM-CL intensity maps were superimposed for the 30 s GRI sample as well (see figure 6(a)). In clear contrast to the 0 s GRI reference sample, the highest panchromatic intensity appears in regions of high dislocation density, exactly where the GaN islands are formed. In figure 6(d), the spectrum integrated over the same area of figure 6(a) exhibits two spectrally separated emission contributions from the GaN layer: one at 218 nm as well as a broad CL band between 230 and 300 nm. The characteristic defect related luminescence of the AlN buffer has been fitted with a Gaussian shape (dashed lines). To identify and visualize the local microscopic origin of the GaN related recombination channels, monochromatic ($\Delta\lambda = 9.6$ nm) STEM-CL intensity images centered at $\lambda = 217$ and 250 nm were recorded. Figure 6(b) clearly reveals the continuous GaN QW as the origin of the 218 nm emission. Complementary to the QW CL intensity image, the 250 nm luminescence in figure 6(c) exhibits the brightest contrast at the very positions of the GaN islands, whereas the QW intensity (see figure 6(b)) drops here. These GaN islands are identified as clusters of GaN QDs formed in the vicinity of TD bundles and are connected by a thin GaN QW (figure 6(d)) (see [18, 19]). These findings are in complete contrast to the reference sample with 0 s GRI (figure 5).

In addition, more detailed structural investigations of the GaN island formation with increasing GRI time were performed in STEM. The cross-sectional HAADF images of the series are displayed in figures 7(a)–(e) (left column). Due to the projection along the electron beam direction, the interpretation of the structural features can be ambiguous. Objects at different TEM film depths but with the same projected image position overlap and are difficult to distinguish. STEM tilt series enable a three-dimensional tomographic illustration. To get an in-plane view of the mass thickness contrast of the islands, the samples were slightly tilted off-axis in figures 7(f)–(j). The reference sample shown in

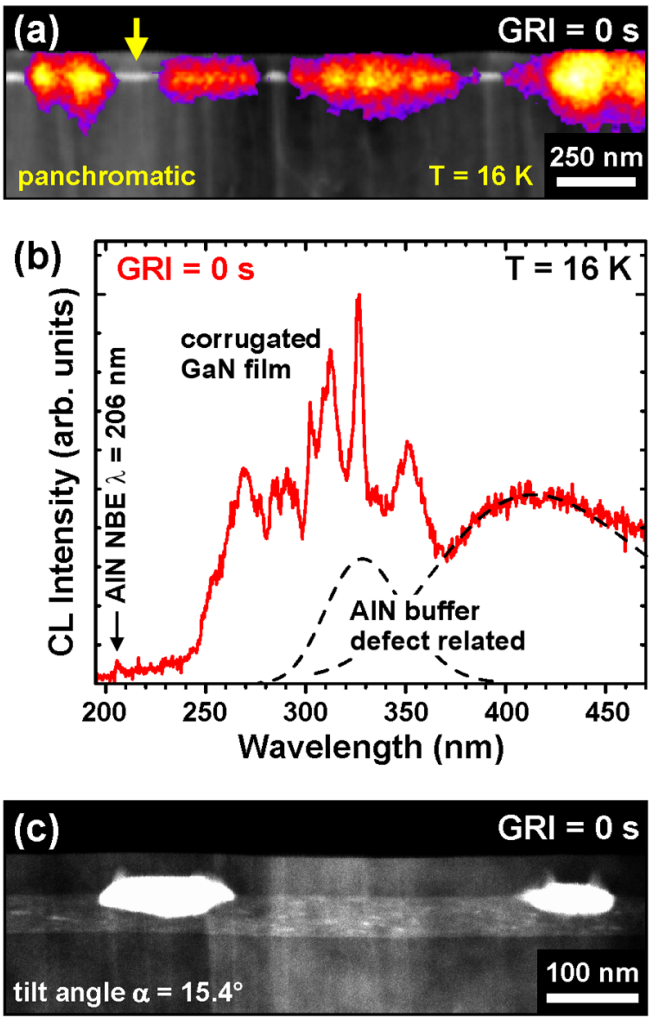

Figure 5. (a) Superposition of panchromatic CL intensity and HAADF image of the sample with no GRI at $T = 16$ K (arrow indicates one GaN island). Exclusively, the corrugated GaN film shows excitonic luminescence between the GaN islands. (b) STEM-CL ensemble spectrum of the same area as displayed in figure 1 reveals a broad emission band between 250 and 360 nm and AlN buffer defect related emission with Gaussian fit (dashed lines) (see also figure 6(d)). (c) Magnified off-axis view of another GaN layer part of the same sample with GaN islands and corrugated GaN film.

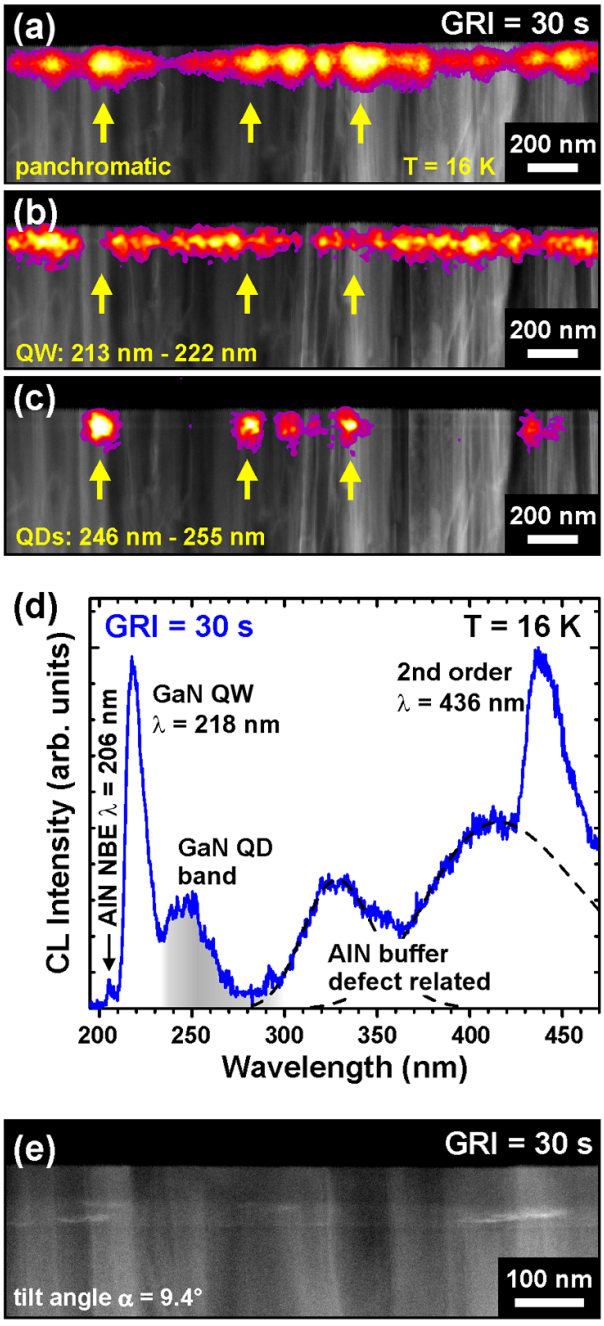

Figure 6. (a) HAADF image of the sample with 30 s GRI time and superposition with panchromatic CL intensity distribution, (b) monochromatic CL intensity distribution at 213–222 nm (QW emission) and (c) monochromatic CL at 246–255 nm (QD emission) (arrows indicate clusters of GaN QDs). (d) STEM-CL spectrum of the 30 s GRI sample with GaN QW emission at 218 nm and a broad emission band between 235 and 300 nm from the GaN QDs (gray faded area) and AlN buffer defect related emission with Gaussian fit (dashed lines). (e) Magnified off-axis view of the GaN layer with clustered GaN QDs and GaN QW.

figures 7(a) and (f) reveal a continuous GaN film (∼2 nm thick) topped with hexagonally shaped, truncated pyramids of 20 nm thickness and ∼100 nm lateral diameter. They were preferentially formed at dislocation bundles. In the case of 5 s GRI, the GaN islands are fragmented and less defined in shape (see figures 7(b) and (g)) with lateral extension up to 350 nm. This indicates an initial material transport during the GRI. Furthermore, the GaN QW thickness is reduced. In the off-axis view only half of the GaN island remained due to sample preparation. In this view, the uprising bundle of TDs below the GaN island is clearly observable. With increasing GRI, further fragmentation of the islands occurs leading to clusters of separated QDs. The height and width of individual QDs decrease down to 4.5 and 20 nm for $t_{GRI} = 30$ s, respectively (see figures 7(d) and (i)). Here, the thickness of the GaN QW reduces to 1–2 monolayers. For longer GRI times, the GaN QW eventually vanishes and only clusters of QDs are observed near TDs (see figures 7(e) and (j)).

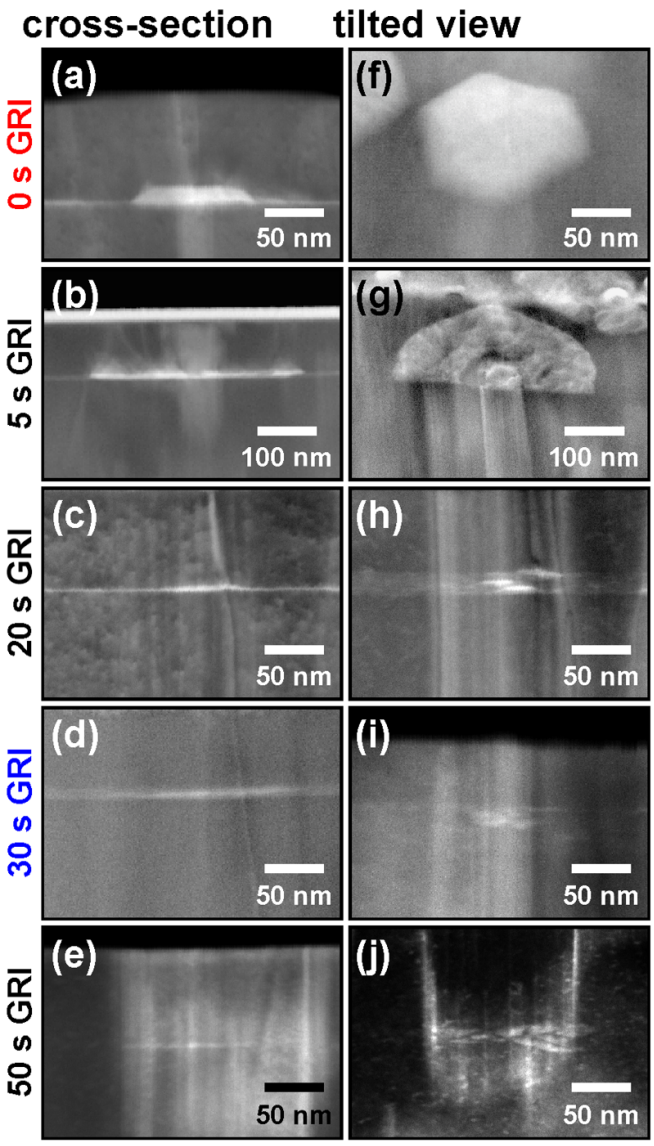

Figure 7. HAADF images of the samples with GRI times (a) and (f) 0 s (reference as in figure 5), (b) and (g) 5 s, (c) and (h) 20 s, (d) and (i) 30 s (as in figure 6) and (e), (j) 50 s in (a)–(e) cross-section view and (f)–(j) off-axis view.

4. Conclusions

The fragmentation and shrinking of island dimensions as well as QW thickness with increasing GRI indicate a GaN desorption process during the GRI. First, bulky compact GaN islands are preferentially formed in close vicinity to bundles of TDs during the MOVPE growth of GaN on top of AlN. The favored accumulation of GaN close to bundles of TDs might be explained by the reduced strain [29] compared to the surrounding lattice mismatch of GaN on AlN [30] or altered surface morphology in general. Here, only luminescence from the corrugated GaN film and no emission from GaN islands at the dislocation bundles is observed. When applying a GRI directly after GaN deposition, GaN desorption occurs and is initially accompanied by lateral material transport. This results in a transition from bulky to fragmented islands or even clustered QDs (for $t_{GRI} > 10$ s). The alteration most likely depends on local strain fields as well as different facet orientation of the island surface and is driven by the temperature inside the growth chamber. This structural transition is accompanied by a drastic change in the luminescence properties. Besides the QW recombination, QD luminescence from islands is observed in complete contrast to the reference sample with no GRI. Here, the radiative recombination of the generated excess carriers within the islands is predominant. Increasing GRI leads to a monotonous decrease of QW thickness as well as island size. In accordance with the structural changes, a systematic blue shift of the QW and QD emission wavelength is observed, verifying the stronger carrier confinement. The QW luminescence disappears for long GRI, when the desorption leads to the vanishing of the QW structure.

In summary, we investigated the formation process of MOVPE grown GaN/AlN QDs and their structural and optical evolution during GRI after an initial GaN deposition step. The GaN QDs result from initially bulky GaN islands due to desorption during GRI. Despite their direct vicinity to TDs, the formed QDs are optically active. Longer GRI leads to smaller dimensions of the quantum heterostructures accompanied by a blue shift of the involved recombination channels, which directly verifies the desorption process. Our analysis of the systematic growth series of self-organized GaN QDs offers the possibility to directly control the QD size by using the GRI time.

Data availability statement

The data that support the findings of this study are available from the corresponding author upon reasonable request.

Acknowledgments

We gratefully acknowledge the German Research Foundation for its financial support in the framework of the Research Instrumentation Program INST 272/148-1 as well as the Collaborative Research Center SFB 787 ‘Semiconductor Nanophotonics: Materials, Models, Devices’. Many thanks are extended to Silke Petzold for her great work regarding the laborious TEM preparations.

Conflict of interest

The authors declare no competing interests.

Author contributions

S M, G S and H S performed SEM-CL and STEM-CL investigations. G S and H S prepared the manuscript. P V assisted characterization with STEM-CL. F B and J C are supervisors of the SEM-CL and STEM-CL equipment. C B performed MOVPE growth while A D and A S built and supervise the MOVPE growth setup. All authors discussed the results and commented on the manuscript.

ORCID iDs

H Schürmann https://orcid.org/0000-0002-6328-670X
G Schmidt https://orcid.org/0000-0002-2524-2116
F Bertram https://orcid.org/0000-0003-2753-7628
A Dadgar https://orcid.org/0000-0002-4174-1169
A Strittmatter https://orcid.org/0000-0002-0519-4882
J Christen https://orcid.org/0000-0001-8689-7004

References

[1] O'Brien J L, Furusawa A and Vučković J 2009 *Nat. Photon.* **3** 687–95
[2] Gisin N and Thew R 2007 *Nat. Photon.* **1** 165–71
[3] de Rinaldis S, D'Amico I, Biolatti E, Rinaldi R, Cingolani R and Rossi F 2002 *Phys. Rev.* B **65** 081309
[4] Imamoglu A 2003 *Physica* E **16** 47–50
[5] Kako S, Santori C, Hoshino K, Götzinger S, Yamamoto Y and Arakawa Y 2006 *Nat. Mater.* **5** 887–92
[6] Holmes M J, Choi K, Kako S, Arita M and Arakawa Y 2014 *Nano Lett.* **12** 982–6
[7] Holmes M J, Kako S, Choi K, Arita M and Arakawa Y 2016 *ACS Photonics* **3** 543–6
[8] Ramvall P, Tanaka S, Nomura S, Riblet P and Aoyagi Y 1998 *Appl. Phys. Lett.* **73** 1104–6
[9] Pohl U W, Rodt S and Hoffmann A 2008 *Semiconductor Nanostructures* ed D Bimberg (Berlin: Springer) p 280
[10] Daudin B, Widmann F, Feuillet G, Samson Y, Arlery M and Rouvière J L 1997 *Phys. Rev.* B **56** R7069–72
[11] Widmann F, Simon J, Daudin B, Feuillet G, Rouvière J L, Pelekanos N T and Fishman G 1998 *J. Appl. Phys.* **83** R15989–92
[12] Adelmann C, Gogneau N, Sarigiannidou E, Rouvière J L and Daudin B 2002 *Appl. Phys. Lett.* **81** 3064
[13] Tanaka S, Iwai S and Aoyagi Y 1996 *Appl. Phys. Lett.* **69** 4096
[14] Miyamura M, Tachibana K and Arakawa Y 2002 *Appl. Phys. Lett.* **80** 3937
[15] Simeonov D, Feltin E, Carlin J-F, Butté R, Ilegems M and Grandjean N 2006 *J. Appl. Phys.* **99** 083509
[16] Zhang J C, Meyler B, Vardi A, Bahir G and Salzman J 2008 *J. Appl. Phys.* **104** 044307
[17] Bellmann K, Tabataba-Vakili F, Wernicke T, Strittmatter A, Callsen G, Hoffmann A and Kneissl M 2015 *Phys. Status Solidi* **9** 526–9
[18] Schmidt G *et al* 2015 *Appl. Phys. Lett.* **106** 252101
[19] Schmidt G, Veit P, Berger C, Bertram F, Dadgar A, Strittmatter A and Christen J 2016 *Jpn. J. Appl. Phys.* **55** 05FF04
[20] Schmidt G *et al* 2020 *Semiconductor Nanophotonics* ed M Kneissl, A Knorr, S Reitzenstein and A Hoffmann (Switzerland: Springer Nature) pp 473–84
[21] Tang Y, Rich D H, Mukhametzhanov I, Chen P and Madhukar A 1998 *J. Appl. Phys.* **84** 3342
[22] Kanaya K and Okayama S 1972 Considering a backscattering of beam electrons of 25% *J. Phys. D: Appl. Phys.* **5** 43–58
[23] Bertram F, Riemann T, Christen J, Kaschner A, Hoffmann A, Thomsen C, Hiramatsu K, Shibata T and Sawaki N 1999 *Appl. Phys. Lett.* **74** 359
[24] Schmidt G, Müller M, Veit P, Bertram F, Christen J, Glauser M, Carlin J-F, Cosendey G, Butté R and Grandjean N 2014 *Appl. Phys. Lett.* **105** 032101
[25] Hartel P, Rose H and Dinges C 1996 *Ultramicroscopy* **63** 93–114
[26] Cowley J M and Huang Y 1992 *Ultramicroscopy* **40** 171
[27] Pastrňák J and Roskovcová L 1966 *Phys. Status Solidi* **14** K5
[28] Bastek B, Bertram F, Christen J, Hempel T, Dadgar A and Krost A 2009 *Appl. Phys. Lett.* **95** 032106
[29] Rouvière J L, Simon J, Pelekanos N, Daudin B and Feuillet G 1999 *Appl. Phys. Lett.* **75** 2632
[30] Kisielowski C *et al* 1996 *Phys. Rev.* B **54** 17745